

Testing the effect of H_0 on $f\sigma_8$ tension using a Gaussian Process method

En-Kun Li,^{*} Minghui Du,[†] Zhi-Huan Zhou,[‡] Hongchao Zhang,[§] Lixin Xu[¶]

Institute of Theoretical Physics, School of Physics, Dalian University of Technology, Dalian, 116024, China

Accepted XXX. Received YYY; in original form ZZZ

ABSTRACT

Using the $f\sigma_8(z)$ redshift space distortion (RSD) data, the $\sigma_8^0 - \Omega_m^0$ tension is studied utilizing a parameterization of growth rate $f(z) = \Omega_m(z)^\gamma$. Here, $f(z)$ is derived from the expansion history $H(z)$ which is reconstructed from the observational Hubble data applying the Gaussian Process method. It is found that different priors of H_0 have great influences on the evolution curve of $H(z)$ and the constraint of $\sigma_8^0 - \Omega_m^0$. When using a larger H_0 prior, the low redshifts $H(z)$ deviate significantly from that of the Λ CDM model, which indicates that a dark energy model different from the cosmological constant can help to relax the H_0 tension problem. The tension between our best-fit values of $\sigma_8^0 - \Omega_m^0$ and that of the *Planck* 2018 Λ CDM (PLA) will disappear (less than 1σ) when taking a prior for H_0 obtained from PLA. Moreover, the tension exceeds 2σ level when applying the prior $H_0 = 73.52 \pm 1.62$ km/s/Mpc resulted from the Hubble Space Telescope photometry. By comparing the $S_8 - \Omega_m^0$ planes of our method with the results from KV450+DES-Y1, we find that using our method and applying the RSD data may be helpful to break the parameter degeneracies.

Key words: method: numerical — methods: statistical — cosmological parameters — large-scale structure of Universe

1 INTRODUCTION

The past and present analyses of various cosmological observations converge to the fact that our Universe is undergoing an accelerated expansion phase (Hicken et al. 2009; Komatsu et al. 2011; Blake et al. 2011; Hinshaw et al. 2013; Farooq et al. 2013; Ade et al. 2016; Aghanim et al. 2020). To explain this phenomenon, two kinds of interpretations have been raised. One is proposing an unknown component with negative pressure called dark energy in the context of General Relativity (GR), and the other is modifying the laws of gravity (MG). Based on these two branches, numerous models have been presented. Among these models, Lambda Cold Dark Matter (Λ CDM) model is the most simple one and can excellently fit with almost all observational data, such as the cosmic microwave background (CMB) radiations (Hinshaw et al. 2013; Ade et al. 2016; Aghanim et al. 2020), the baryon acoustic oscillations (BAO) (Percival et al. 2007; Delubac et al. 2015; Alam et al. 2017; Ruggeri et al. 2019), and the type Ia Supernovae (SNIa) (Perlmutter et al. 1999;

Riess et al. 1998; Suzuki et al. 2012; Betoule et al. 2014), etc.

Nonetheless, it is becoming exceedingly apparent that there are some discrepancies between the *Planck* Λ CDM results and some independent observations in intermediate cosmological scale (Raveri 2016). These discrepancies include the estimates of the Hubble constant H_0 (Ferreira et al. 2017; Bernal et al. 2016; Huang & Wang 2016; Solà et al. 2017; Riess et al. 2018, 2019), the matter density parameter Ω_m^0 and the amplitude of the power spectrum on the scale of $8h^{-1}\text{Mpc}$ (σ_8^0) (Gao & Gong 2014; Battye et al. 2015; Bull et al. 2016; Solà Peracaula et al. 2018; McCarthy et al. 2018), etc. In order to solve these discrepancies, different methods and cosmology models have been reported, including viscous bulk cosmology (Mostaghel et al. 2017), assuming a variable Newton constant (Nesseris et al. 2017; Kazantzidis & Perivolaropoulos 2018), considering the interaction between neutrinos and dark matter (Di Valentino et al. 2018), introducing interacting dark energy (Di Valentino et al. 2017; Yang et al. 2018), model-independent method (Zhao et al. 2017; Gómez-Valent & Amendola 2018; Li et al. 2020), and so on.

Precise large-scale structure measurements are helpful to distinguish different models because these models may have different growth histories of structure. As a starting point, in the subhorizon ($k \gg aH$), the equation that de-

* E-mail: ekli_091@mail.dlut.edu.cn

† E-mail: angelbeats@mail.dlut.edu.cn

‡ E-mail: scott@mail.dlut.edu.cn

§ E-mail: zhanghc@mail.dlut.edu.cn

¶ Corresponding author: lxxu@dlut.edu.cn

scribes the evolution of the linear matter growth factor $\delta = \delta\rho_m/\rho_m$ in the context of GR and most MG models has the form (Kazantzidis & Perivolaropoulos 2018)

$$\delta'' + \left(\frac{H'}{H} - \frac{1}{1+z} \right) \delta' \simeq \frac{3}{2}(1+z) \frac{H_0^2}{H^2} \frac{G_{\text{eff}}(z,k)}{G_N} \Omega_m^0 \delta, \quad (1)$$

where ρ_m is the background matter density, $H = \dot{a}/a$ is the Hubble expansion rate at scale factor $a = 1/(1+z)$, G_N is the Newton's constant, G_{eff} is the effective Newton's constant which in general may depend on both the redshift z and the cosmological scale k , and “ $'$ ” denotes a derivative with respect to z . In GR we have $G_{\text{eff}} = G_N$ while in MG G_{eff}/G_N may vary with both cosmological redshift and scale.

Although it is difficult to give the analytical solution of Eq. (1), a good parameterization of the growth rate $f(a) \equiv d\ln\delta/d\ln a$ is given by (Wang & Steinhardt 1998; Amendola & Quercellini 2004; Linder 2005; Polarski & Gannouji 2008; Gannouji & Polarski 2008; Polarski et al. 2016; Nesseris & Sapone 2015)

$$f(a) \simeq \Omega_m(a)^\gamma, \quad (2)$$

where $\Omega_m(a) = \Omega_m^0 a^{-3}/(H(a)/H_0)^2$ is the fractional matter density, and γ is the growth index. The growth index differs between different cosmological models (Xu 2013; Polarski et al. 2016). In the Λ CDM model, $\gamma = 6/11$ is a solution to Eq. (1) where the terms $\mathcal{O}(1 - \Omega_m(a))^2$ are neglected (Wang & Steinhardt 1998), while $\gamma \simeq 0.55$ is that of dark energy models with slowly varying equation of state (Linder 2005). For MG models, different values are predicted, e.g., $\gamma \simeq 0.68$ for Dvali-Gabadadze-Porrati (DGP) braneworld model (Linder & Cahn 2007; Wei 2008). Applying some model-independent methods, authors in Refs. (L'Huillier et al. 2018; Shafieloo et al. 2018; L'Huillier et al. 2019) found that the value of γ is consistent with that of the flat- Λ CDM model, and Yin & Wei (Yin & Wei 2019a,b) also investigated the time varying $\gamma(z)$. Since most of the information on linear clustering is expected to come from the epoch of equality of matter and dark energy, it is reasonable to use this parameterization to approximate $f(z)$ (Pogosian et al. 2010).

In particular, most of the growth rate measurements can be obtained from redshift space distortion (RSD) measurements via the peculiar velocities of galaxies (Kaiser 1987). However, $f(z)$ is sensitive to the bias parameter b , which makes the observation of $f(z)$ data unreliable (Nesseris et al. 2017). Therefore, most growth rate measurements are reported as the combination $f(z)\sigma_8(z) = f\sigma_8(z)$ instead of $f(z)$, where $\sigma_8(z) = \sigma_8^0 \delta(z)/\delta_0$ is the matter power spectrum normalization on scales of $8h^{-1}$ Mpc. In addition, the joint measurement of expansion history and growth history provides an important test of GR and can help to break the degeneracies between MG theories and dark energy models in GR (Linder 2005, 2017). In this paper, using the RSD data and the observational Hubble data (OHD), we will investigate the $\sigma_8^0 - \Omega_m^0$ tension utilizing the Gaussian Process method. We reconstruct the expansion history $H(z)$ firstly using the OHD data with priors for Hubble constant H_0 , and then derive the theoretical value of $f\sigma_8(z)$ applying the parameterization $f(z) = \Omega_m(z)^\gamma$. Finally, by adopting the Markov Chain Monte Carlo (MCMC) method, the constraints on the free parameters in $f\sigma_8(z)$ are given using the RSD data corrected by the fiducial model corrections.

The layout of this work is as follows. In section 2, we introduce the basic methodology adopted to derive $f\sigma_8(z)$ and the observational data combinations used to constrain free parameters. And then, in section 3, we show the reconstruction of Hubble parameter $H(z)$ and $f\sigma_8(z)$ under different combinations of OHD. Our results and discussions are displayed in section 4. At last, we summarize our conclusions in section 5.

2 METHODOLOGY AND OBSERVATIONAL DATA

2.1 Methodology

As we known that most growth rate measurements are reported as the combination $f\sigma_8(z)$. Using the definitions of $f(z)$, $\sigma_8(z)$ and Eq. (2), one can obtain

$$f\sigma_8(z) = \sigma_8^0 (\Omega_m^0 H_0^2)^\gamma \left(\frac{(1+z)^3}{H(z)^2} \right)^\gamma \cdot \exp \left[-(\Omega_m^0 H_0^2)^\gamma \int_0^z \frac{(1+z')^{3\gamma-1}}{H(z')^{2\gamma}} dz' \right]. \quad (3)$$

Thus, given an expansion history function $H(z)$ or $H(z)/H_0$, we can reconstruct the observable quantity $f\sigma_8(z)$, assuming σ_8^0 , Ω_m^0 and γ are known.

The Gaussian Process method (Rasmussen & Williams 2006; Seikel et al. 2012; Seikel & Clarkson 2013) can provide a smooth reconstructed $H(z)$ using the combination of OHD without assuming a parametrisation of the function. So we can get a full model-independent reconstructed $f\sigma_8(z)$ with three free parameters $\{\sigma_8^0, \Omega_m^0, \gamma\}$ using Eq. (3).

Now, we can use a χ^2 minimization to constrain the three free parameters,

$$\chi^2 = \Delta \mathbf{V}^T \mathbf{Cov}^{-1} \Delta \mathbf{V}, \quad (4)$$

$$\Delta V_i = f\sigma_{8,\text{obs}}(z_i) - f\sigma_{8,\text{rec}}(z_i) \quad (5)$$

$$\mathbf{Cov} = \mathbf{Cov}^{\text{obs}} + \mathbf{Cov}^{\text{rec}}, \quad (6)$$

where $\mathbf{Cov}^{\text{obs}}$ is the covariance matrix of $f\sigma_{8,\text{obs}}$ and $\mathbf{Cov}^{\text{rec}}$ is the covariance matrix of the reconstructed $f\sigma_{8,\text{rec}}(z)$ which is defined in Eq. (3). The likelihood of the free parameters can be obtained from $\mathcal{L} \propto \exp[-\chi^2/2]$. The constraints on the free parameters are performed using the Markov Chain Monte Carlo (MCMC) sampling method. It's easy to do this by using the publicly available code Cobaya¹, which calls the MCMC sampler developed for CosmoMC (Lewis & Bridle 2002; Lewis 2013).

Furthermore, in order to quantify the tension between different estimate of parameter ξ , we need to introduce a quantization function of the tension level. Assuming the 68% confidence level ranges of parameter ξ is $\xi \in [\xi_1 - \sigma_{1,\text{low}}, \xi_1 + \sigma_{1,\text{up}}]$ from observation O_1 , and $\xi \in [\xi_2 - \sigma_{2,\text{low}}, \xi_2 + \sigma_{2,\text{up}}]$ from observation O_2 . Then, the simplest and most intuitive way to measure the degree of tension can be written as (Zhao et al. 2018)

$$s \equiv \frac{\xi_1 - \xi_2}{\sqrt{\sigma_{1,\text{low}}^2 + \sigma_{2,\text{up}}^2}}, \quad (7)$$

for the case $\xi_1 > \xi_2$. This means that the tension of ξ between O_1 and O_2 is at $s\sigma$ level.

¹ <https://github.com/CobayaSampler/cobaya>

2.2 $f\sigma_8(z)$ measurements

Table A1 shows a sample consisting of 63 observational $f\sigma_{8,\text{obs}}(z)$ RSD data points collected by Kazantzidis & Perivolaropoulos (2018). It comprises the data published by various surveys from 2006 to the present and the parameters of the corresponding fiducial cosmology model are also shown in this table. For more details please refer to Ref. (Kazantzidis & Perivolaropoulos 2018) and references therein.

The covariance matrix of the 63 $f\sigma_8$ data points are assumed to be diagonal except for the WiggleZ subset of the data (three data points). The covariance matrix of the three points of WiggleZ has been published as

$$C_{i,j}^{\text{WiggleZ}} = 10^{-3} \times \begin{pmatrix} 6.400 & 2.570 & 0.000 \\ 2.570 & 3.969 & 2.540 \\ 0.000 & 2.540 & 5.184 \end{pmatrix}. \quad (8)$$

One should note that all the $f\sigma_{8,\text{obs}}(z)$ data listed in Table A1 are obtained assuming a fiducial Λ CDM cosmology (Kazantzidis & Perivolaropoulos 2018). Thus, the Alcock-Paczynski (AP) effect (Alcock & Paczynski 1979) should be considered. In the present paper, we will use the following rough approximation of the AP effect (Macaulay et al. 2013; Kazantzidis & Perivolaropoulos 2018)

$$f\sigma_{8,\text{ap}}(z) \simeq \frac{H(z)D_A(z)}{H^{\text{fid}}(z, \Omega_m)D_A^{\text{fid}}(z, \Omega_m)} f\sigma_{8,\text{obs}}(z), \quad (9)$$

where $D_A(z)$ is the angular diameter distance, and it can be written as

$$D_A(z) = \frac{c}{1+z} \int_0^z \frac{dz'}{H(z')}, \quad (10)$$

in the spatially flat universe.

2.3 Observational Hubble data

The Hubble parameter $H(z)$ is usually evaluated as a function of the redshift z

$$H(z) = -\frac{1}{1+z} \frac{dz}{dt}. \quad (11)$$

It can be seen that $H(z)$ depends on the derivative of redshift with respect to cosmic time. The $H(z)$ measurements can be obtained via two approaches. One is calculating the differential ages of passively evolving galaxies (Jimenez & Loeb 2002) providing $H(z)$ measurements that are model-independent. This method is usually called the cosmic chronometers (CC). The other method is based on the clustering of galaxies or quasars, which is firstly proposed by (Gaztanaga et al. 2009), where the BAO peak position is used as a standard ruler in the radial direction.

Here, we use the compilation of OHD data points collected by Magana, et al. (Magana et al. 2018) and Geng, et al. (Geng et al. 2018), including almost all $H(z)$ data reported in various surveys so far. The 31 CC $H(z)$ data points are listed in Table A2 and the 23 $H(z)$ data points obtained from clustering measurements are listed in Table A3. One may find that some of the $H(z)$ data points from clustering measurements are correlated since they either belong to the same analysis or there is overlap between the galaxy samples. Here in this paper, we mainly take the central value and standard deviation of the OHD data into consideration.

Thus, just as in Ref. (Geng et al. 2018), we assume that they are independent measurements.

In addition, there is no observation for H_0 in these OHD data points mentioned above, so we also consider two different priors of H_0 . One is $H_0 = 67.27 \pm 0.60$ km/s/Mpc (Aghanim et al. 2020) provided by *Planck 2018* power spectra (TT,TE,EE+lowE) measurements by assuming base Λ CDM model (hereafter P18). The other is $H_0 = 73.52 \pm 1.62$ km/s/Mpc presented by the Hubble Space Telescope photometry of long-period Milky Way Cepheids and GAIA parallaxes (Riess et al. 2018) (hereafter R18).

3 MODEL-INDEPENDENT RECONSTRUCTION

GP method provides a technique to reconstruct a function using the observational data without assuming a specific parameterization. It is easy to reconstruct the Hubble parameters directly from the OHD data applying a freely available GaPP package². The numerical program written by ourselves is used in this paper, and there is no difference between our code and that of GaPP, which also indicates our program is credible.

GP are characterized by mean and covariance functions, which are defined by a small number of hyperparameters. Throughout this work, we assume a priori mean function equal to zero, and use the squared exponential covariance function:

$$k(x, y) = \sigma_f^2 \exp\left(-\frac{(x-y)^2}{2l^2}\right), \quad (12)$$

where σ_f and l are two hyperparameters which can be determined by the observational data. Supposing an observational data-set $\{x_i, y_i, \sigma_i\}$, where x_i is the location of data point i , $y_i = f(x_i) + \epsilon_i$ is the corresponding actual observed value which is assumed to be scattered around the underlying function $f(x_i)$ and Gaussian noise with variance σ_i is assumed. Using the GP method, the reconstructed mean value and covariance of the underlying function $f(x)$ can be written as (Seikel et al. 2012)

$$f(x) = \sum_{i,j=1}^N k(x, x_i)(M^{-1})_{ij}y_i, \quad (13)$$

$$\text{Cov}(f_x, f_y) = k(x, y) - \sum_{i,j=1}^N k(x, x_i)(M^{-1})_{ij}k(x_j, y), \quad (14)$$

where $M_{ij} = k(x_i, x_j) + C_{ij}$ and C_{ij} is the covariance matrix of the observational data.

3.1 Reconstruction of Hubble parameter

By using Eqs. (13) and (14), one can easily get the reconstructed Hubble parameters $H(z)$ and its covariance matrix between different redshifts. The propagated covariance (Alam et al. 2004; Nesseris & Perivolaropoulos 2005; Wang & Xu 2010; Xu 2013) of the reconstructed $E(z)$ can be calculated with the reconstructed $H(z)$, and its covariance matrix

² <http://www.acgc.uct.ac.za/~seikel/GAPP/index.html>

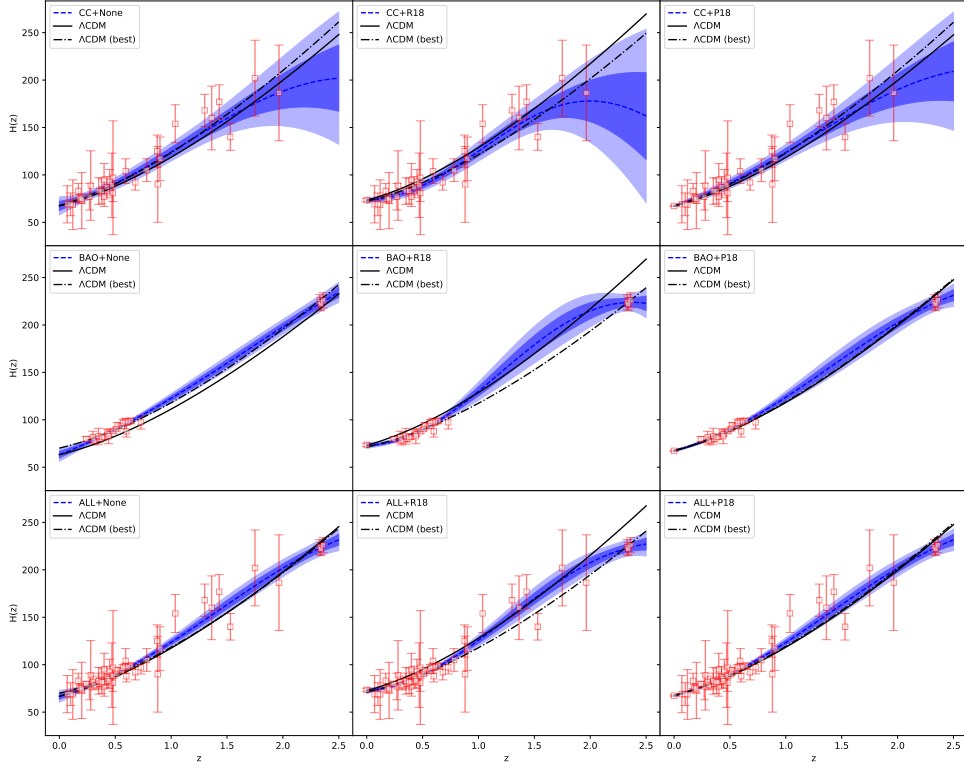


Figure 1. The blue region is the reconstructed $H(z)$ as function of redshift z within 2σ confidence level. The solid black lines represent the Λ CDM model with $\Omega_m = 0.3$ and H_0 is the reconstructed mean value from the corresponding data combinations. The dot dashed lines are the Λ CDM model using the mean values of the model parameters from Table 1. The red error bar plot is OHD data.

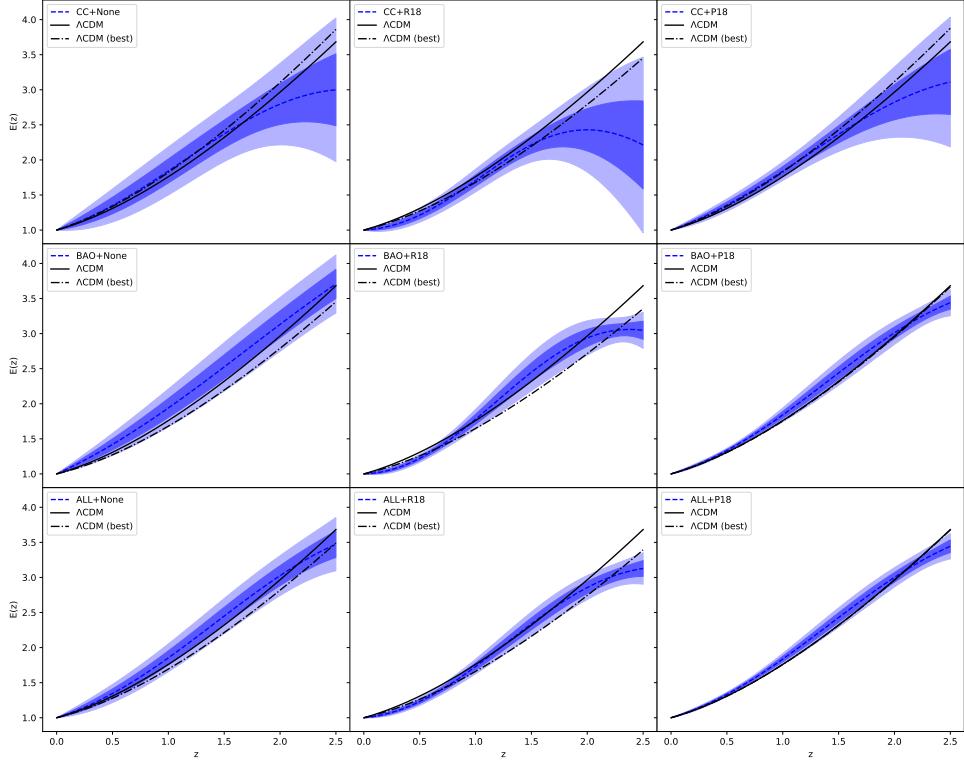


Figure 2. The reconstructed $E(z)$ as function of redshift z within 2σ region. The solid black lines are the Λ CDM model with $\Omega_m = 0.3$. The dot dashed lines are the Λ CDM model using the mean values of the model parameters from Table 1.

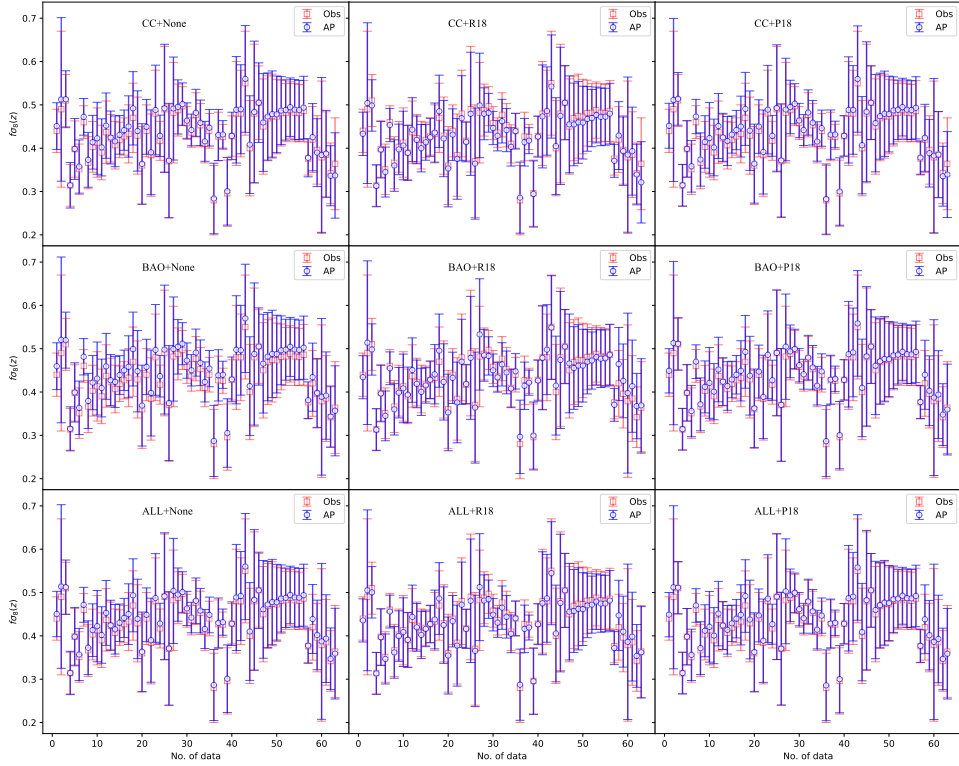


Figure 3. Here the index ‘‘Obs’’ is for the original data and ‘‘AP’’ is the data after fiducial model correction. The $f\sigma_8^{ap}(z)$ data in different graphs are obtained with different reconstructions of $H(z)$.

is

$$\begin{aligned} \text{Cov}[E_i, E_j] = & E_i E_j \left(\frac{\text{Cov}[H_i, H_j]}{H_i H_j} - \frac{\text{Cov}[H_i, H_0]}{H_i H_0} \right. \\ & \left. - \frac{\text{Cov}[H_0, H_j]}{H_0 H_j} + \frac{\text{Cov}[H_0, H_0]}{H_0 H_0} \right) \end{aligned} \quad (15)$$

where $E_i = E(z_i) = H(z_i)/H_0$ is the dimensionless Hubble parameter, and $H_i = H(z_i)$ is the reconstructed Hubble parameter at z_i .

Next, we will examine the differences between the reconstructed $H(z)$ under various OHD data combinations. In Figs. 1 and 2, we have plotted the reconstructed $H(z)$ and $E(z)$ within 2σ region using different data combinations, and the reconstructed H_0 is also listed in Table 1. Here the indexes CC, BAO and ALL represent the OHD data obtained from CC, clustering measurements, and CC+clustering measurements, respectively. We also consider three different priors of H_0 , i.e., no prior (index None), H_0 of R18 and H_0 of P18. The three panels of the first column in Figs. 1 and 2 are the reconstructed results from the three data combinations with no prior on H_0 . From the values of H_0 listed in Table 1, one may find that OHD from BAO prefers a much smaller H_0 than P18 or R18, and the mean value of the derived H_0 from the CC data is much close to that of P18. However, we should note that the tension level of the three reconstructed H_0 with P18 or R18 are all less than 2σ as a result of the big error bars.

Comparing the three panels in the same rows of Figs. 1 and 2, one can find that adding a prior on H_0 can significantly reduce the error bars of the reconstructed $H(z)$ at low redshifts, because the H_0 measurements of R18 and P18

have much smaller variances than the rest OHD data points. It also can be found that the slope of the reconstructed $H(z)$ varies when choosing different priors of H_0 , especially at low redshifts $z < 0.5$. For the cases of using the same OHD data points but with different H_0 priors, we find that the evolution curves of $H(z)$ under the P18 prior are similar to that without H_0 prior, this is due to the fact that they have similar mean values of H_0 .

Meanwhile, from Figs. 1 and 2, we can see that CC data gives a much looser reconstruction of $H(z)$ at higher redshifts than BAO data, which is because the BAO data points have much smaller variances at high redshifts. And the Λ CDM model with fixed Ω_m and the mean values from the constraint results in Table 1 are also shown in the two figures as comparison. One can also find that when the R18 prior is taken into consideration, our reconstructions are much different with the Λ CDM model.

3.2 $f\sigma_8(z)$ data after fiducial model correction

In this work, we will use the reconstructed model-independent $H(z)$ and $D_A(z)$ for fiducial model correction. Thus, the central value of $f\sigma_8^{ap}(z)$ and its covariance matrix can be calculated according to Eq. (9). The covariance matrix will be

$$\text{Cov}_{ij}^{ap} = q_i q_j \text{Cov}_{ij}^* + p_i p_j \text{Cov}_{ij}^{HD}, \quad (16)$$

where Cov^* and Cov^{HD} are the covariance of observational RSD data and the reconstructed $H(z)D_A(z)$, respectively, $q_i = H_i D_{A,i} / (H_i^{\text{fid}} D_{A,i}^{\text{fid}})$, and $p_i = f\sigma_{8,i,\text{obs}} / (H_i^{\text{fid}} D_{A,i}^{\text{fid}})$.

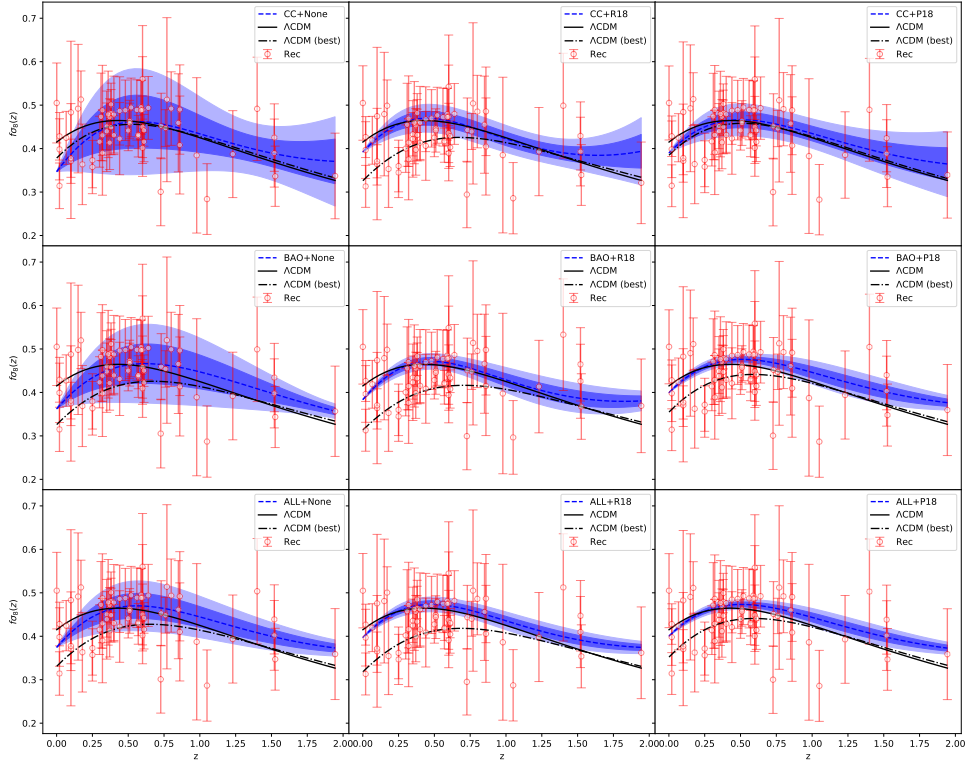


Figure 4. The blue region is the reconstruction of $f\sigma_8(z)$ using the reconstructed $H(z)$ from OHD data through Eq. (17) within 2σ region, the dot dashed lines are $f\sigma_8(z)$ derived from Eq. (3) under ΛCDM model with different parameters. The red error bar plot are the measurements of RSD data after fiducial model correction. The parameters used here are the mean values from Table 1. For comparison, the ΛCDM model with the fixed parameters: $\Omega_m = 0.3$, $\sigma_8 = 0.8$, and $\gamma = 0.545$ are also shown in every panels (solid black lines).

The original $f\sigma_{8,\text{obs}}(z)$ data and the fiducial model correction data $f\sigma_{8,\text{ap}}(z)$ are plotted in Fig. 3. As shown in Fig. 3 this correction has little effect on the mean values of $f\sigma_8(z)$. After some calculations, we find that the largest corrections on the mean values and the variances are less than 11% and 18%, respectively. The correlations between different data points also need to be taken into account when constraining on the free parameters.

3.3 Reconstruction of $f\sigma_8(z)$

Using the reconstructed $H(z)$ or $E(z)$, the reconstructed $f\sigma_8(z)$ can be obtained through Eq. (3). The mean value and the propagated covariance (Alam et al. 2004; Nesseris & Perivolaropoulos 2005; Wang & Xu 2010; Xu 2013) of the reconstructed $f\sigma_8(z)$ can be written as

$$f\sigma_8(z_i) = \sigma_8^0(\Omega_m^0)^\gamma \frac{(1+z)^{3\gamma}}{E^{2\gamma}(z)} \exp [-(\Omega_m^0)^\gamma I_i], \quad (17)$$

$$\begin{aligned} \text{Cov}[f\sigma_{8,i}, f\sigma_{8,j}] &= 4\gamma^2 f\sigma_{8,i} f\sigma_{8,j} \left\{ \frac{\text{Cov}[E_i, E_j]}{E_i E_j} \right. \\ &\quad \left. - (\Omega_m^0)^\gamma M_{ij} - (\Omega_m^0)^\gamma M_{ji} + (\Omega_m^0)^{2\gamma} N_{ij} \right\}, \end{aligned} \quad (18)$$

where $f\sigma_{8,i} = f\sigma_8(z_i)$,

$$I_i = \int_0^{z_i} \frac{(1+z)^{3\gamma-1}}{E^{2\gamma}(z)} dz, \quad (19)$$

$$M_{ij} = \int_0^{z_j} \frac{(1+z)^{3\gamma-1}}{H^{2\gamma}(z)} \frac{\text{Cov}[E(z), E_i]}{E(z) E_i} dz, \quad (20)$$

$$N_{ij} = \int_0^{z_i} \int_0^{z_j} \frac{[(1+x)(1+y)]^{3\gamma-1}}{[E(x)E(y)]^{2\gamma}} \frac{\text{Cov}[E(x), E(y)]}{E(x)E(y)} dx dy. \quad (21)$$

In Fig. 4, we plot the variation of $f\sigma_8(z)$ reconstructed under different data combinations with respect to redshift z . As shown in this figure, the uncertainties of the reconstructed $f\sigma_8(z)$ from BAO or CC+BAO data combination are much smaller than the observational uncertainties, which is due to the smaller variances of $H(z)$ from BAO data can significantly reduce the reconstructed errors of $f\sigma_8(z)$ at high redshifts.

One can find that the when the R18 prior are considered, the slopes of the reconstructed $f\sigma_8(z)$ varies greatly. These changes are consistent with the reconstruction of $H(z)$ described in section 3.1.

4 RESULTS AND DISCUSSION

In this section, we describe the main results acquired from the model-independent method considered in this work. As a comparison, we also give constrain on the ΛCDM model under the OHD and the RSD data points³. The flat-

³ For ΛCDM model, the parameterization of $f = \Omega_m(z)^\gamma$ are also used to constrain on cosmological parameters. And the constraint results of ΛCDM model are given under the combination of OHD data and $f\sigma_8(z)$ data.

Table 1. 68% and 95% confidence level constraints on the free parameters for various observational data combinations. Note that H_0 of the GP method is directly reconstructed from the OHD data. Here “ALL” correspond to the data combination of “CC+BAO”.

Method	Data combination	σ_8^0	Ω_m^0	γ	S_8	H_0 [km/s/Mpc]
GP	RSD+CC+None	$0.703_{-0.16}^{+0.057} < 0.969$	$0.46_{-0.10}^{+0.16+0.23}$	$0.91_{-0.19}^{+0.19+0.38}$	$0.829_{-0.039}^{+0.045+0.089}$	$67.36 \pm 4.8 \pm 9.6$
	RSD+CC+R18	$0.92_{-0.24}^{+0.13+0.42} < 0.380$	$0.169_{-0.15}^{+0.057} < 0.380$	$0.48_{-0.13}^{+0.10+0.23}$	$0.603_{-0.052}^{+0.15+0.18}$	$73.24 \pm 1.6 \pm 3.2$
	RSD+CC+P18	$0.754_{-0.19}^{+0.068} < 1.07$	$0.41_{-0.13}^{+0.19+0.27}$	$0.74_{-0.17}^{+0.17+0.34}$	$0.815_{-0.014}^{+0.062+0.10}$	$67.26 \pm 0.60 \pm 1.20$
	RSD+BAO+None	$0.719_{-0.16}^{+0.061+0.27} < 0.22$	$0.507_{-0.095}^{+0.16+0.23}$	$1.01_{-0.20}^{+0.20+0.38}$	$0.900_{-0.041}^{+0.048+0.085}$	$63.22 \pm 3.4 \pm 6.8$
	RSD+BAO+R18	$1.14_{-0.19}^{+0.19} > 0.828$	$0.095_{-0.077}^{+0.023+0.13}$	$0.463_{-0.099}^{+0.079+0.18}$	$0.579_{-0.082}^{+0.14+0.19}$	$73.15 \pm 1.6 \pm 3.2$
	RSD+BAO+P18	$0.92_{-0.25}^{+0.12+0.43} < 0.32$	$0.26_{-0.18}^{+0.11+0.25}$	$0.62_{-0.15}^{+0.13+0.27}$	$0.772_{-0.026}^{+0.10+0.12}$	$67.22 \pm 0.59 \pm 1.18$
	RSD+ALL+None	$0.86_{-0.23}^{+0.10+0.40} < 0.31$	$0.32_{-0.14}^{+0.14+0.25}$	$0.73_{-0.18}^{+0.15+0.32}$	$0.817_{-0.022}^{+0.068+0.11}$	$66.68 \pm 3.1 \pm 6.2$
	RSD+ALL+R18	$1.04_{-0.26}^{+0.18+0.41} < 0.34$	$0.123_{-0.11}^{+0.035} < 0.300$	$0.460_{-0.11}^{+0.083+0.21}$	$0.594_{-0.067}^{+0.15+0.19}$	$72.62 \pm 1.5 \pm 3.0$
Λ CDM	RSD+ALL+P18	$0.91_{-0.25}^{+0.12+0.42} < 0.33$	$0.26_{-0.18}^{+0.11+0.25}$	$0.61_{-0.15}^{+0.13+0.30}$	$0.766_{-0.022}^{+0.10+0.13}$	$67.25 \pm 0.59 \pm 1.18$
	RSD+CC+None	$0.80_{-0.15}^{+0.13+0.25}$	$0.332_{-0.070}^{+0.051+0.13}$	$0.68_{-0.32}^{+0.28+0.56}$	$0.84_{-0.20}^{+0.14+0.35}$	$67.7_{-3.1}^{+3.1+5.9}$
	RSD+CC+R18	$0.78_{-0.15}^{+0.12+0.24}$	$0.261_{-0.032}^{+0.032+0.066}$	$0.65_{-0.33}^{+0.28+0.56}$	$0.73_{-0.15}^{+0.12+0.26}$	$72.2 \pm 1.4 \pm 2.8$
	RSD+CC+P18	$0.80_{-0.15}^{+0.12+0.25}$	$0.335_{-0.032}^{+0.032+0.064}$	$0.67_{-0.32}^{+0.27+0.56}$	$0.84_{-0.16}^{+0.13+0.28}$	$67.31_{-0.59}^{+0.59+1.1}$
	RSD+BAO+None	$0.78_{-0.15}^{+0.12+0.24}$	$0.261_{-0.020}^{+0.017+0.040}$	$0.65_{-0.32}^{+0.28+0.55}$	$0.73 \pm 0.11_{-0.21}^{+0.22}$	$70.2_{-1.2}^{+1.2+2.3}$
	RSD+BAO+R18	$0.77_{-0.15}^{+0.12+0.24}$	$0.245_{-0.015}^{+0.015+0.030}$	$0.64_{-0.33}^{+0.27+0.56}$	$0.69_{-0.13}^{+0.10+0.23}$	$71.31_{-0.93}^{+0.93+1.8}$
	RSD+BAO+P18	$0.79_{-0.15}^{+0.12+0.24}$	$0.297_{-0.012}^{+0.012+0.025}$	$0.66_{-0.28}^{+0.28+0.54}$	$0.81 \pm 0.13_{-0.23}^{+0.25}$	$67.83_{-0.55}^{+0.55+1.1}$
	RSD+ALL+None	$0.78_{-0.15}^{+0.12+0.24}$	$0.267_{-0.019}^{+0.017+0.035}$	$0.65_{-0.32}^{+0.28+0.55}$	$0.76 \pm 0.13_{-0.24}^{+0.25}$	$69.9_{-1.1}^{+1.1+2.1}$
	RSD+ALL+R18	$0.77_{-0.15}^{+0.11+0.24}$	$0.251_{-0.014}^{+0.014+0.029}$	$0.64_{-0.33}^{+0.27+0.55}$	$0.72_{-0.14}^{+0.11+0.25}$	$71.01_{-0.90}^{+0.90+1.7}$
	RSD+ALL+P18	$0.79_{-0.15}^{+0.12+0.25}$	$0.299_{-0.012}^{+0.012+0.023}$	$0.67_{-0.33}^{+0.28+0.56}$	$0.79_{-0.14}^{+0.12+0.26}$	$67.86 \pm 0.53 \pm 1.0$

linear priors for the free parameters we choose are $\sigma_8^0 \in [0.5, 1.5]$, $\Omega_m^0 \in [0.0, 1.0]$, and $\gamma \in [0.0, 1.5]$. For the Λ CDM model, we choose $H_0 \in [55, 90]$ and the priors of the other three parameters are the same as that of the GP method.

The summary of the observational constraints on the free parameters using different data combinations is listed in Table 1. The results show that in the Λ CDM model, the different OHD data combinations and different priors of H_0 have little influence on σ_8^0 and γ , but have significant impacts on Ω_m^0 and H_0 . Unlike that in the Λ CDM model, the various data combinations and the priors of H_0 have great influence on the constraints of all the free parameters of the GP method.

In Table 1, one can find that the Λ CDM model gives a much tighter constraint on H_0 than the GP method, this is because that, in the GP method, H_0 is reconstructed using only the OHD data. By comparing our results of the Λ CDM model with the PLA results, where $\sigma_8^0 = 0.8120 \pm 0.0073$ and $\Omega_m^0 = 0.3166 \pm 0.0084$ (Aghanim et al. 2020), we find that σ_8^0 is consistent with the PLA results in 1σ region under different data combinations with or without prior on H_0 . Meanwhile, all the constraints of γ in Λ CDM model are consistent with the GR prediction $\gamma = 0.55$ in 1σ region.

From Table 1, we note that in the Λ CDM model and the GP reconstruction method, the increasing of H_0 results in a decreasing of Ω_m^0 , which increases the tension level between our constraint Ω_m^0 and that of the PLA results. To better understand the relationship and tension level between the free parameters, in Figs. 5, 6 and 7 we display the 2-D

contour plots and the 1-D posterior distributions of the corresponding free parameters under different cases. From the 1-D posterior distributions and the values in Table 1, one can find that in the GP method, the Hubble constant H_0 is smaller than that in the Λ CDM model when applying None or P19 prior on H_0 , while Ω_m^0 is larger and σ_8^0 is lower. However, when a prior R18 is considered, we find the opposite trend.

The contour plots of the GP method in the three figures suggest that σ_8^0 is anti-correlated with Ω_m^0 and γ , but Ω_m^0 is positively correlated with γ , which are quite different from that of Λ CDM model. As can be seen from Figs. 5–7 and the results in Table 1, the OHD data from BAO prefers larger σ_8^0 , Ω_m^0 and γ than the CC data if we do not take any prior on H_0 . However, using all the OHD data points without prior on H_0 , the best-fit of our results are closer to that of PLA results than using only OHD data from CC or BAO. Comparing the results under the same data combination, it can be found that the three free parameters vary greatly under different priors of H_0 , especially the matter density parameter Ω_m^0 , which suggests that H_0 has a great influence on constraining the three parameters.

From the $\Omega_m^0 - \sigma_8^0$ contour plots in Figs. 5, 6 and 7, one can find that the tension level between our constraint $\Omega_m^0 - \sigma_8^0$ and the PLA values are within 1σ level when taking P18 H_0 prior and out of 2σ level when taking R18 prior. The dashed lines in the $\Omega_m^0 - \sigma_8^0$ contour plots represent the best-fit values of PLA results. On the other hand, the tension is often quantified using the $S_8 \equiv \sigma_8^0 \sqrt{\Omega_m^0}/0.3$ pa-

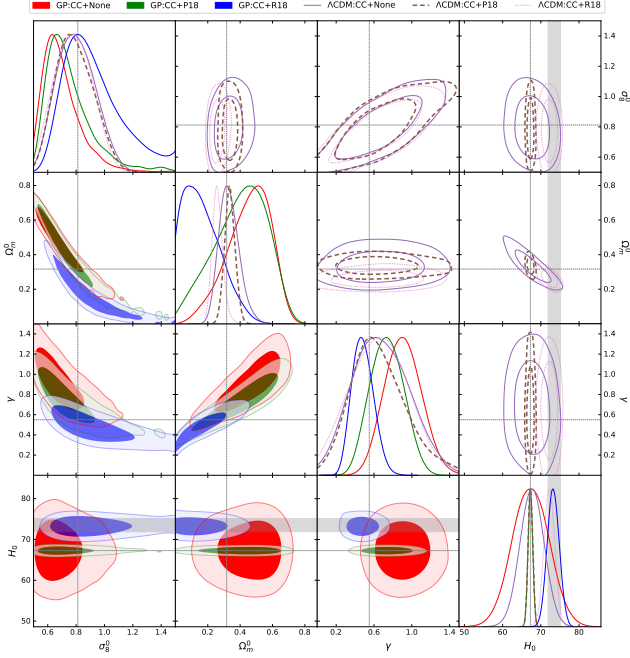


Figure 5. The 68% and 95% confidence level contour plots of the free parameters and the corresponding one dimensional marginalized posterior distributions under the RSD+CC data combination. The vertical and horizontal dotted lines represent $\sigma_8^0 = 0.8120$, $\Omega_m^0 = 0.3166$, $\gamma = 0.545$ and $H_0 = 67.27$. The grey vertical band corresponds to the R18 value.

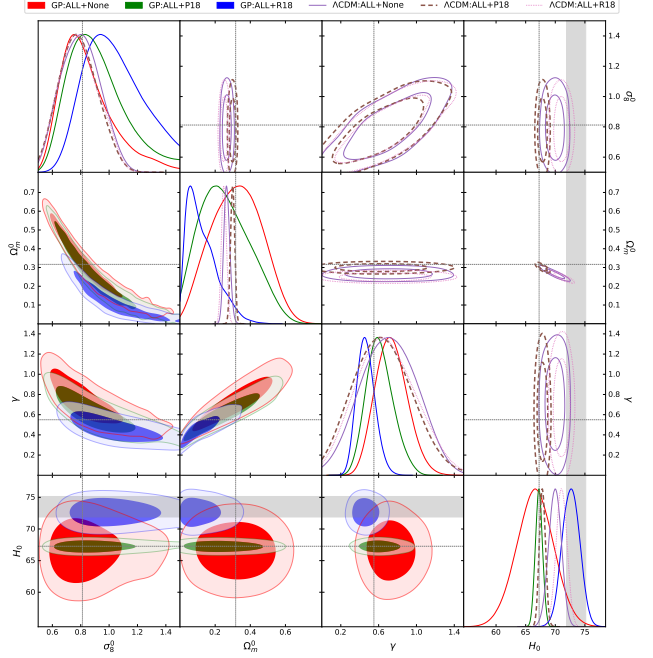


Figure 7. The 68% and 95% confidence level contour plots of the free parameters and the corresponding one dimensional marginalized posterior distributions under the RSD+ALL data combination.. The vertical and horizontal dotted lines represent $\sigma_8^0 = 0.8120$, $\Omega_m^0 = 0.3166$, $\gamma = 0.545$ and $H_0 = 67.27$. The grey vertical band corresponds to the R18 value.

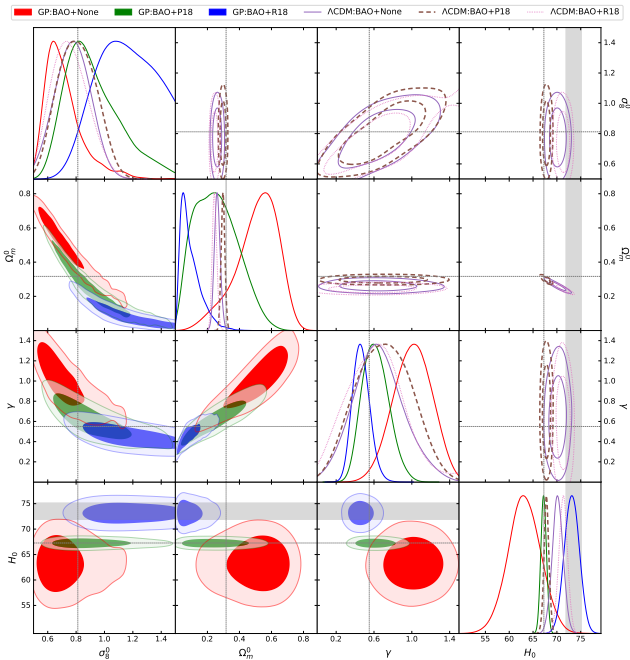


Figure 6. The 68% and 95% confidence level contour plots of the free parameters and the corresponding one dimensional marginalized posterior distributions under the RSD+BAO data combination.. The vertical and horizontal dotted lines represent $\sigma_8^0 = 0.8120$, $\Omega_m^0 = 0.3166$, $\gamma = 0.545$ and $H_0 = 67.27$. The grey vertical band corresponds to the R18 value.

parameter, along the main degeneracy direction of weak lensing measurements (Di Valentino et al. 2020). Thus, the contour plots of $S_8 - \Omega_m^0$ of different cases are shown in Fig. 8 - 10. In the $S_8 - \Omega_m^0$ planes, the result from KV450 and DES-Y1 measurements (Joudaki et al. 2020) are plotted as a contrast. From these contourplots, one can find that the correlations between S_8 and Ω_m^0 are quite different between GP method and Λ CDM model. One can also find that S_8 is positively correlated with Ω_m^0 in our methods, which is different with the KV450+DES-Y1 results. This suggest that our methods are helpful in breaking the degeneracies of the two parameters if the KV450 and DES-Y1 data are considered. Meanwhile, from the contours, one can obtain that the difference of S_8 in the GP method is less than 2σ with PLA results when applying None and P19 priors of H_0 . But when the R19 prior are applied, the tension is bigger than 2σ .

Besides, though our constrainton the growth index γ varies greatly in different cases, the tension level between our constraint result and the GR prediction are almost less than 2σ .

5 SUMMARY

In this work, we consider the constraints on the matter fluctuation amplitude σ_8^0 , the matter density parameter Ω_m^0 , and the growth index γ by using the latest OHD and RSD data combinations. To be model-independent, we use GP method to reconstruct the Hubble parameter $H(z)$ from different OHD data combinations, and then obtain a theoretical $f\sigma_8(z)$ function. We then use the reconstructed $f\sigma_8(z)$

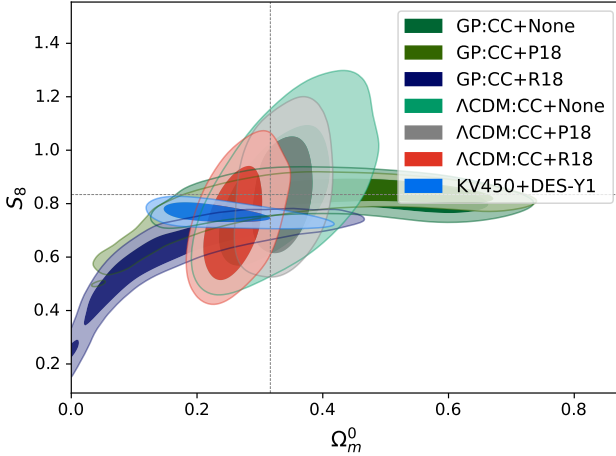


Figure 8. 68% and 95% confidence level contour plots for S_8 and Ω_m^0 under RSD+CC data. The vertical and horizontal dotted lines represent $S_8 = 0.834$ and $\Omega_m^0 = 0.3166$ from PLA results.

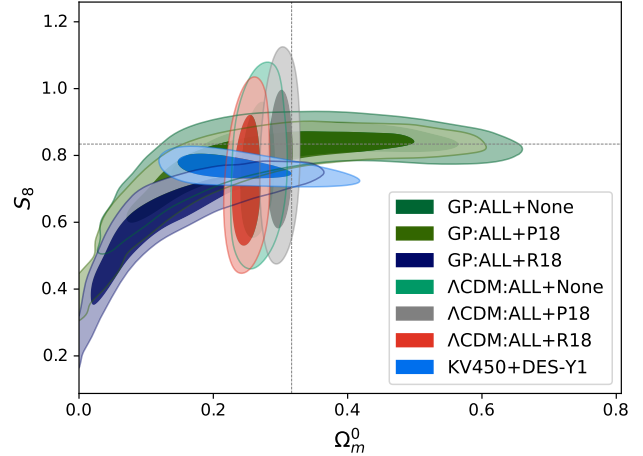


Figure 10. 68% and 95% confidence level contour plots for S_8 and Ω_m^0 under RSD+ALL data. The vertical and horizontal dotted lines represent $S_8 = 0.834$ and $\Omega_m^0 = 0.3166$ from PLA results.

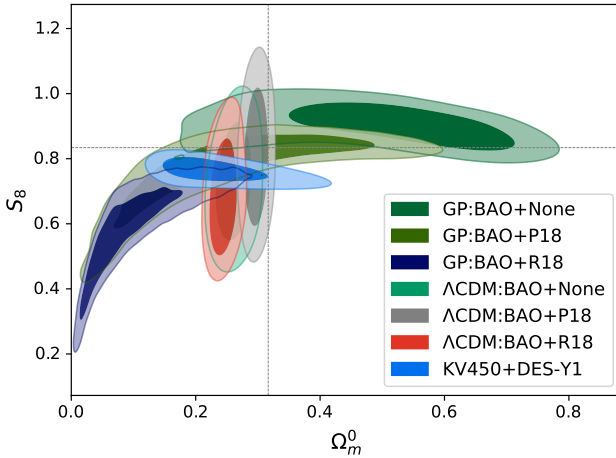


Figure 9. 68% and 95% confidence level contour plots for S_8 and Ω_m^0 under RSD+BAO data. The vertical and horizontal dotted lines represent $S_8 = 0.834$ and $\Omega_m^0 = 0.3166$ from PLA results.

and the RSD data to sample the free parameters by means of the MCMC method. Here, to reduce the impact of the AP effect, we also correct the RSD data using the $H(z)$ and $D_A(z)$ reconstructed by GP method.

From the curves of the reconstructed $H(z)$ and $E(z)$ shown in Figs. 1 and 2 respectively, one can find that the expansion history varies greatly from the Λ CDM model when taking R18 prior on H_0 , especially at the low redshifts. This indicates that to solve or relax the H_0 tension problem, it is necessary to have a model with a different expansion history from the Λ CDM model or a dynamical dark energy model which is different from the cosmological constant at low redshifts.

As in Fig. 4, the reconstructed $f\sigma_8(z)$ fits well with the Λ CDM model when using the same cosmological parameters. Meanwhile, we also find that both the expansion history $H(z)$ and the prior of H_0 have great influences on the

reconstruction of the $f\sigma_8(z)$, which is also supported by the MCMC sampling results obtained in this paper.

Our results show that the tension level between our best-fit of $\Omega_m^0 - \sigma_8^0$ and that of the PLA results are no more than 2σ in the cases of no H_0 prior. And the tension will even disappear (because of less than 1σ) when adopting P18 H_0 prior. This conclusion are also supported by the $S_8 - \Omega_m^0$ contour plots. Meanwhile, the different correlations between our results and the KV450+DES-Y1 results suggest that using our method and combine the RSD and OHD data may be helpful to break the $S_8 - \Omega_m^0$ degeneracies in cosmic shear measurements. However, one should note that our constraints on Ω_m^0 and σ_8^0 are much looser compared with the PLA results, which means that the small tension level may be caused by the larger uncertainties. Nonetheless, using all the OHD data points and the RSD data without H_0 prior, our constraint result of Ω_m^0 and σ_8^0 are very close to the PLA values, and the tension level between the growth index γ and the GR prediction $\gamma = 0.55$ is at 1σ level.

From our analysis, one can find that the mean values of H_0 have a great influence on the reconstructed expanding history $H(z)$, the reconstructed growth history $f\sigma_8(z)$, and the constraint results of cosmological parameters. Compared with R18, Riess et al. (2019) present an even larger value of H_0 , i.e., 74.03 ± 1.42 km/s/Mpc (R19). Thus, if this value is chosen as H_0 prior, the reconstructed $H(z)$ will be much bigger at low redshifts. According to the results shown in Table 1, H_0 is positively-correlated with σ_8^0 and anti-correlated with Ω_m^0 and γ , thus, if the R19 is used, we will get a larger σ_8^0 but smaller Ω_m^0 and γ .

It should be noted that the possibility of correlations exists in the $f\sigma_8$ datapoints are not considered in the present paper. Kazantzidis & Perivolaropoulos (2018) had considered positive correlations in 12 randomly selected pairs of the 63 $f\sigma_8(z)$ datapoints. They find that the introduction of a nontrivial covariance matrix does not change the qualitative conclusions of their analysis of the tensions. So in this paper, we only take the correlation matrix generated from the fiducial model corrections (see section 3.2).

ACKNOWLEDGMENTS

This work is supported in part by National Natural Science Foundation of China under Grant No. 11675032 and Grant No. 12075042 (People's Republic of China). E.-K. Li thanks J. Geng for suggestions of English language revising.

DATA AVAILABILITY

The data underlying this article are available in the article and the references details can be found in the APPENDIX A.

REFERENCES

- Ade P. A. R., et al., 2016, *Astron. Astrophys.*, 594, A13
 Aghanim N., et al., 2020, *Astron. Astrophys.*, 641, A6
 Alam U., Sahni V., Saini T. D., Starobinsky A. A., 2004, arXiv:astro-ph/0406672
 Alam S., et al., 2017, *Mon. Not. Roy. Astron. Soc.*, 470, 2617
 Alcock C., Paczynski B., 1979, *Nature*, 281, 358
 Amendola L., Quercellini C., 2004, *Phys. Rev. Lett.*, 92, 181102
 Anderson L., Aubourg E., Bailey S., Beutler F., Bhardwaj V., Blanton M., Bolton A. S., et al., 2014, *Mon. Not. Roy. Astron. Soc.*, 441, 24
 Battye R. A., Charnock T., Moss A., 2015, *Phys. Rev. D*, 91, 103508
 Bautista J. E., Busca N. G., Guy J., Rich J., Blomqvist M., Bourboux H. D. M. D., Pieri M. M., et al., 2017, *Astron. Astrophys.*, 603, A12
 Bernal J. L., Verde L., Riess A. G., 2016, *JCAP*, 1610, 019
 Betoule M., et al., 2014, *Astron. Astrophys.*, 568, A22
 Beutler F., et al., 2012, *Mon. Not. Roy. Astron. Soc.*, 423, 3430
 Beutler F., Seo H.-J., Saito S., Chuang C.-H., Cuesta A. J., Eisenstein D. J., Gil-Marín H., et al., 2017, *Mon. Not. Roy. Astron. Soc.*, 466, 2242
 Blake C., et al., 2011, *Mon. Not. Roy. Astron. Soc.*, 418, 1707
 Blake C., et al., 2012, *Mon. Not. Roy. Astron. Soc.*, 425, 405
 Blake C., et al., 2013, *Mon. Not. Roy. Astron. Soc.*, 436, 3089
 Bull P., et al., 2016, *Phys. Dark Univ.*, 12, 56
 Chuang C.-H., Wang Y., 2013, *Mon. Not. Roy. Astron. Soc.*, 435, 255
 Chuang C.-H., Prada F., Pellejero-Ibanez M., Beutler F., Cuesta A. J., Eisenstein D. J., et al., 2016, *Mon. Not. Roy. Astron. Soc.*, 461, 3781
 Davis M., Nusser A., Masters K., Springob C., Huchra J. P., Lemson G., 2011, *Mon. Not. Roy. Astron. Soc.*, 413, 2906
 De La Torre S., et al., 2013, *Astron. Astrophys.*, 557, A54
 De La Torre S., et al., 2017, *Astron. Astrophys.*, 608, A44
 Delubac T., et al., 2015, *Astron. Astrophys.*, 574, A59
 Di Valentino E., Melchiorri A., Mena O., 2017, *Phys. Rev. D*, 96, 043503
 Di Valentino E., Bøehm C., Hivon E., Bouchet F. R., 2018, *Phys. Rev. D*, 97, 043513
 Di Valentino E., et al., 2020, arXiv:2008.11285
 Farooq O., Mania D., Ratra B., 2013, *Astrophys. J.*, 764, 138
 Feix M., Nusser A., Branchini E., 2015, *Phys. Rev. Lett.*, 115, 011301
 Feix M., Branchini E., Nusser A., 2017, *Mon. Not. Roy. Astron. Soc.*, 468, 1420
 Ferreira E. G. M., Quintin J., Costa A. A., Abdalla E., Wang B., 2017, *Phys. Rev. D*, 95, 043520
 Font-Ribera A., Kirkby D., Busca N., Miralda-Escudé J., Ross N. P., Slosar A., Rich J., et al., 2014, *JCAP*, 1405, 027
 Gannouji R., Polarski D., 2008, *JCAP*, 0805, 018
 Gao Q., Gong Y., 2014, *Class. Quant. Grav.*, 31, 105007
 Gaztanaga E., Cabre A., Hui L., 2009, *Mon. Not. Roy. Astron. Soc.*, 399, 1663
 Geng J.-J., Guo R.-Y., Wang A., Zhang J.-F., Zhang X., 2018, *Commun. Theor. Phys.*, 70, 445
 Gil-Marín H., et al., 2018, *Mon. Not. Roy. Astron. Soc.*, 477, 1604
 Gil-Marín H., Percival W. J., Verde L., Brownstein J. R., Chuang C.-H., Kitaura F.-S., Rodríguez-Torres S. A., Olmstead M. D., 2017, *Mon. Not. Roy. Astron. Soc.*, 465, 1757
 Gómez-Valent A., Amendola L., 2018, *JCAP*, 1804, 051
 Hawken A. J., et al., 2017, *Astron. Astrophys.*, 607, A54
 Hicken M., Wood-Vasey W. M., Blondin S., Challis P., Jha S., Kelly P. L., Rest A., Kirshner R. P., 2009, *Astrophys. J.*, 700, 1097
 Hinshaw G., et al., 2013, *Astrophys. J. Suppl.*, 208, 19
 Hou J., Sánchez A. G., Scoccimarro R., Salazar-Albornoz S., Burtin E., Gil-Marín H., Percival W. J., et al., 2018, *Mon. Not. Roy. Astron. Soc.*, 480, 2521
 Howlett C., Ross A., Samushia L., Percival W., Manera M., 2015, *Mon. Not. Roy. Astron. Soc.*, 449, 848
 Howlett C., et al., 2017, *Mon. Not. Roy. Astron. Soc.*, 471, 3135
 Huang Q.-G., Wang K., 2016, *Eur. Phys. J. C*, 76, 506
 Hudson M. J., Turnbull S. J., 2013, *Astrophys. J.*, 751, L30
 Huterer D., Shafer D., Scolnic D., Schmidt F., 2017, *JCAP*, 1705, 015
 Jimenez R., Loeb A., 2002, *Astrophys. J.*, 573, 37
 Joudaki S., et al., 2020, *Astron. Astrophys.*, 638, L1
 Kaiser N., 1987, *Mon. Not. Roy. Astron. Soc.*, 227, 1
 Kazantzidis L., Perivolaropoulos L., 2018, *Phys. Rev. D*, 97, 103503
 Komatsu E., et al., 2011, *Astrophys. J. Suppl.*, 192, 18
 L'Huillier B., Shafieloo A., Kim H., 2018, *Mon. Not. Roy. Astron. Soc.*, 476, 3263
 L'Huillier B., Shafieloo A., Polarski D., Starobinsky A. A., 2020, *Mon. Not. Roy. Astron. Soc.*, 494, 819
 Lewis A., 2013, *Phys. Rev. D*, 87, 103529
 Lewis A., Bridle S., 2002, *Phys. Rev. D*, 66, 103511
 Li E.-K., Du M., Xu L., 2020, *Monthly Notices of the Royal Astronomical Society*, 491, 4960
 Linder E. V., 2005, *Phys. Rev. D*, 72, 043529
 Linder E. V., 2017, *Astropart. Phys.*, 86, 41
 Linder E. V., Cahn R. N., 2007, *Astropart. Phys.*, 28, 481
 Macaulay E., Wehus I. K., Eriksen H. K., 2013, *Phys. Rev. Lett.*, 111, 161301
 Magana J., Amante M. H., Garcia-Aspeitia M. A., Motta V., 2018, *Mon. Not. Roy. Astron. Soc.*, 476, 1036
 McCarthy I. G., Bird S., Schaye J., Harnois-Deraps J., Font A. S., Van Waerbeke L., 2018, *Mon. Not. Roy. Astron. Soc.*, 476, 2999
 Mohammad F. G., et al., 2018, *Astron. Astrophys.*, 610, A59
 Moresco M., 2015, *Mon. Not. Roy. Astron. Soc.*, 450, L16
 Moresco M., et al., 2012, *JCAP*, 1208, 006
 Moresco M., et al., 2016, *JCAP*, 1605, 014
 Mostaghel B., Moshafi H., Movahed S. M. S., 2017, *Eur. Phys. J. C*, 77, 541
 Nesseris S., Perivolaropoulos L., 2005, *Phys. Rev. D*, 72, 123519
 Nesseris S., Sapone D., 2015, *Phys. Rev. D*, 92, 023013
 Nesseris S., Pantazis G., Perivolaropoulos L., 2017, *Phys. Rev. D*, 96, 023542
 Oka A., Saito S., Nishimichi T., Taruya A., Yamamoto K., 2014, *Mon. Not. Roy. Astron. Soc.*, 439, 2515
 Okumura T., Hikage C., Totani T., Tonegawa M., Okada H., Glazebrook K., Blake C., et al., 2016, *Publ. Astron. Soc. Jap.*, 68, 38
 Percival W. J., Cole S., Eisenstein D. J., Nichol R. C., Peacock J. A., Pope A. C., Szalay A. S., 2007, *Mon. Not. Roy. Astron. Soc.*, 381, 1053
 Perlmutter S., et al., 1999, *Astrophys. J.*, 517, 565

- Pezzotta A., et al., 2017, *Astron. Astrophys.*, 604, A33
 Pogosian L., Silvestri A., Koyama K., Zhao G.-B., 2010, *Phys. Rev. D*, 81, 104023
 Polarski D., Gannouji R., 2008, *Phys. Lett. B*, 660, 439
 Polarski D., Starobinsky A. A., Giacomini H., 2016, *JCAP*, 1612, 037
 C. E. Rasmussen & C. K. I. Williams, Gaussian Processes for Machine Learning, the MIT Press, 2006
 Ratsimbazafy A. L., Loubser S. I., Crawford S. M., Cress C. M., Bassett B. A., Nichol R. C., Väistönen P., 2017, *Mon. Not. Roy. Astron. Soc.*, 467, 3239
 Raveri M., 2016, *Phys. Rev. D*, 93, 043522
 Riess A. G., Filippenko A. V., Challis P., Clocchiatti A., Diercks A., Garnavich P. M., Gilliland R. L., et al., 1998, *Astron. J.*, 116, 1009
 Riess A. G., Casertano S., Yuan W., Macri L., Bucciarelli B., Lattanzi M. G., Mackenty J. W., et al., 2018, *Astrophys. J.*, 861, 126
 Riess A. G., Casertano S., Yuan W., Macri L. M., Scolnic D., 2019, *Astrophys. J.*, 876, 85
 Ruggeri R., et al., 2019, *Mon. Not. Roy. Astron. Soc.*, 483, 3878
 Samushia L., Percival W. J., Raccanelli A., 2012, *Mon. Not. Roy. Astron. Soc.*, 420, 2102
 Sanchez A. G., et al., 2014, *Mon. Not. Roy. Astron. Soc.*, 440, 2692
 Seikel M., Clarkson C., 2013, arXiv:1311.6678
 Seikel M., Clarkson C., Smith M., 2012, *JCAP*, 1206, 036
 Shafieloo A., L'Huillier B., Starobinsky A. A., 2018, *Phys. Rev. D*, 98, 083526
 Shi F., et al., 2018, *Astrophys. J.*, 861, 137
 Solà Peracaula J., Perez J. d. C., Gomez-Valent A., 2018, *Mon. Not. Roy. Astron. Soc.*, 478, 4357
 Solà J., Giómez-Valent A., de Cruz Pérez J., 2017, *Astrophys. J.*, 836, 43
 Song Y.-S., Percival W. J., 2009, *JCAP*, 0910, 004
 Stern D., Jimenez R., Verde L., Kamionkowski M., Stanford S. A., 2010, *JCAP*, 1002, 008
 Suzuki N., et al., 2012, *Astrophys. J.*, 746, 85
 Tegmark M., et al., 2004, *Astrophys. J.*, 606, 702
 Tegmark M., et al., 2006, *Phys. Rev. D*, 74, 123507
 Tojeiro R., Percival W. J., Brinkmann J., Brownstein J. R., Eisenstein D. J., Manera M., Maraston C., et al., 2012, *Mon. Not. Roy. Astron. Soc.*, 424, 2339
 Turnbull S. J., Hudson M. J., Feldman H. A., Hicken M., Kirshner R. P., Watkins R., 2012, *Mon. Not. Roy. Astron. Soc.*, 420, 447
 Wang L.-M., Steinhardt P. J., 1998, *Astrophys. J.*, 508, 483
 Wang Y., Xu L., 2010, *Phys. Rev. D*, 81, 083523
 Wang Y., Zhao G.-B., Chuang C.-H., Ross A. J., Percival W. J., Gil-Marín H., Cuesta A. J., et al., 2017, *Mon. Not. Roy. Astron. Soc.*, 469, 3762
 Wang Y., Zhao G.-B., Chuang C.-H., Pellejero-Ibanez M., Zhao C., Kitaura F.-S., Rodriguez-Torres S., 2018, *Mon. Not. Roy. Astron. Soc.*, 481, 3160
 Wei H., 2008, *Phys. Lett. B*, 664, 1
 Wilson M. J., 2016, PhD thesis, Edinburgh U., Edinburgh (arXiv:1610.08362)
 Xu L., 2013, *Phys. Rev. D*, 88, 084032
 Yang W., Pan S., Di Valentino E., Nunes R. C., Vagnozzi S., Mota D. F., 2018, *JCAP*, 1809, 019
 Yin Z.-Y., Wei H., 2019a, *Sci. China Phys. Mech. Astron.*, 62, 999811
 Yin Z.-Y., Wei H., 2019b, *Eur. Phys. J. C*, 79, 698
 Zhang C., Zhang H., Yuan S., Zhang T.-J., Sun Y.-C., 2014, *Res. Astron. Astrophys.*, 14, 1221
 Zhao G.-B., et al., 2017, *Nat. Astron.*, 1, 627
 Zhao M.-M., Zhang J.-F., Zhang X., 2018, *Phys. Lett. B*, 779, 473
 Zhao G.-B., et al., 2019, *Mon. Not. Roy. Astron. Soc.*, 482, 3497

APPENDIX A: $F\sigma_8$ GROWTH DATA AND OBSERVATIONAL HUBBLE DATA COMBINATIONS

This paper has been typeset from a TeX/LaTeX file prepared by the author.

Table A1. A compilation of RSD data that reported in different surveys.

Index	Dataset	z	$f\sigma_8(z)$	Refs.	Year	Fiducial Cosmology
1	SDSS-LRG	0.35	0.440 ± 0.050	[1]	30 October 2006	$(\Omega_{0m}, \Omega_K, \sigma_8 [2]) = (0.25, 0, 0.756)$
2	VVDS	0.77	0.490 ± 0.18	[1]	6 October 2009	$(\Omega_{0m}, \Omega_K, \sigma_8) = (0.25, 0, 0.78)$
3	2dFGRS	0.17	0.510 ± 0.060	[1]	6 October 2009	$(\Omega_{0m}, \Omega_K) = (0.3, 0, 0.9)$
4	2MRS	0.02	0.314 ± 0.048	[3], [4]	13 November 2010	$(\Omega_{0m}, \Omega_K, \sigma_8) = (0.266, 0, 0.65)$
5	SnIa+IRAS	0.02	0.398 ± 0.065	[5], [4]	20 October 2011	$(\Omega_{0m}, \Omega_K, \sigma_8) = (0.3, 0, 0.814)$
6	SDSS-LRG-200	0.25	0.3512 ± 0.0583	[6]	9 December 2011	$(\Omega_{0m}, \Omega_K, \sigma_8) = (0.276, 0, 0.8)$
7	SDSS-LRG-200	0.37	0.4602 ± 0.0378	[6]	9 December 2011	
8	SDSS-LRG-60	0.25	0.3665 ± 0.0601	[6]	9 December 2011	
9	SDSS-LRG-60	0.37	0.4031 ± 0.0586	[6]	9 December 2011	
10	WiggleZ	0.44	0.413 ± 0.080	[7]	12 June 2012	$(\Omega_{0m}, h, \sigma_8) = (0.27, 0.71, 0.8)$
11	WiggleZ	0.60	0.390 ± 0.063	[7]	12 June 2012	$C_{ij} = E_{ij}$ (Eq. (8))
12	WiggleZ	0.73	0.437 ± 0.072	[7]	12 June 2012	
13	6dFGS	0.067	0.423 ± 0.055	[8]	4 July 2012	$(\Omega_{0m}, \Omega_K, \sigma_8) = (0.27, 0, 0.76)$
14	SDSS-BOSS	0.30	0.407 ± 0.055	[9]	11 August 2012	$(\Omega_{0m}, \Omega_K, \sigma_8) = (0.25, 0, 0.804)$
15	SDSS-BOSS	0.40	0.419 ± 0.041	[9]	11 August 2012	
16	SDSS-BOSS	0.50	0.427 ± 0.043	[9]	11 August 2012	
17	SDSS-BOSS	0.60	0.433 ± 0.067	[9]	11 August 2012	
18	Vipers	0.80	0.470 ± 0.080	[10]	9 July 2013	$(\Omega_{0m}, \Omega_K, \sigma_8) = (0.25, 0, 0.82)$
19	SDSS-DR7-LRG	0.35	0.429 ± 0.089	[11]	8 August 2013	$(\Omega_{0m}, \Omega_K, \sigma_8 [12]) = (0.25, 0, 0.809)$
20	GAMA	0.18	0.360 ± 0.090	[13]	22 September 2013	$(\Omega_{0m}, \Omega_K, \sigma_8) = (0.27, 0, 0.8)$
21	GAMA	0.38	0.440 ± 0.060	[13]	22 September 2013	
22	BOSS-LOWZ	0.32	0.384 ± 0.095	[14]	17 December 2013	$(\Omega_{0m}, \Omega_K, \sigma_8) = (0.274, 0, 0.8)$
23	SDSS DR10 and DR11	0.32	0.48 ± 0.10	[14]	17 December 2013	$(\Omega_{0m}, \Omega_K, \sigma_8 [15]) = (0.274, 0, 0.8)$
24	SDSS DR10 and DR11	0.57	0.417 ± 0.045	[14]	17 December 2013	
25	SDSS-MGS	0.15	0.490 ± 0.145	[16]	30 January 2015	$(\Omega_{0m}, h, \sigma_8) = (0.31, 0.67, 0.83)$
26	SDSS-veloc	0.10	0.370 ± 0.130	[17]	16 June 2015	$(\Omega_{0m}, \Omega_K, \sigma_8 [18]) = (0.3, 0, 0.89)$
27	FastSound	1.40	0.482 ± 0.116	[19]	25 November 2015	$(\Omega_{0m}, \Omega_K, \sigma_8 [20]) = (0.27, 0, 0.82)$
28	SDSS-CMASS	0.59	0.488 ± 0.060	[21]	8 July 2016	$(\Omega_{0m}, h, \sigma_8) = (0.307115, 0.6777, 0.8288)$
29	BOSS DR12	0.38	0.497 ± 0.045	[22]	11 July 2016	$(\Omega_{0m}, \Omega_K, \sigma_8) = (0.31, 0, 0.8)$
30	BOSS DR12	0.51	0.458 ± 0.038	[22]	11 July 2016	
31	BOSS DR12	0.61	0.436 ± 0.034	[22]	11 July 2016	
32	BOSS DR12	0.38	0.477 ± 0.051	[23]	11 July 2016	$(\Omega_{0m}, h, \sigma_8) = (0.31, 0.676, 0.8)$
33	BOSS DR12	0.51	0.453 ± 0.050	[23]	11 July 2016	
34	BOSS DR12	0.61	0.410 ± 0.044	[23]	11 July 2016	
35	Vipers v7	0.76	0.440 ± 0.040	[24]	26 October 2016	$(\Omega_{0m}, \sigma_8) = (0.308, 0.8149)$
36	Vipers v7	1.05	0.280 ± 0.080	[24]	26 October 2016	
37	BOSS LOWZ	0.32	0.427 ± 0.056	[25]	26 October 2016	$(\Omega_{0m}, \Omega_K, \sigma_8) = (0.31, 0, 0.8475)$
38	BOSS CMASS	0.57	0.426 ± 0.029	[25]	26 October 2016	
39	Vipers	0.727	0.296 ± 0.0765	[26]	21 November 2016	$(\Omega_{0m}, \Omega_K, \sigma_8) = (0.31, 0, 0.7)$
40	6dFGS+SNIa	0.02	0.428 ± 0.0465	[27]	29 November 2016	$(\Omega_{0m}, h, \sigma_8) = (0.3, 0.683, 0.8)$
41	Vipers	0.6	0.48 ± 0.12	[28]	16 December 2016	$(\Omega_{0m}, \Omega_b, n_s, \sigma_8 [29]) = (0.3, 0.045, 0.96, 0.831)$
42	Vipers	0.86	0.48 ± 0.10	[28]	16 December 2016	
43	Vipers PDR-2	0.60	0.550 ± 0.120	[30]	16 December 2016	$(\Omega_{0m}, \Omega_b, \sigma_8) = (0.3, 0.045, 0.823)$
44	Vipers PDR-2	0.86	0.400 ± 0.110	[30]	16 December 2016	
45	SDSS DR13	0.1	0.48 ± 0.16	[31]	22 December 2016	$(\Omega_{0m}, \sigma_8 [18]) = (0.25, 0.89)$
46	2MTF	0.001	0.505 ± 0.085	[32]	16 June 2017	$(\Omega_{0m}, \sigma_8) = (0.3121, 0.815)$
47	Vipers PDR-2	0.85	0.45 ± 0.11	[33]	31 July 2017	$(\Omega_b, \Omega_{0m}, h) = (0.045, 0.30, 0.8)$
48	BOSS DR12	0.31	0.469 ± 0.098	[34]	15 September 2017	$(\Omega_{0m}, h, \sigma_8) = (0.307, 0.6777, 0.8288)$
49	BOSS DR12	0.36	0.474 ± 0.097	[34]	15 September 2017	
50	BOSS DR12	0.40	0.473 ± 0.086	[34]	15 September 2017	
51	BOSS DR12	0.44	0.481 ± 0.076	[34]	15 September 2017	
52	BOSS DR12	0.48	0.482 ± 0.067	[34]	15 September 2017	
53	BOSS DR12	0.52	0.488 ± 0.065	[34]	15 September 2017	
54	BOSS DR12	0.56	0.482 ± 0.067	[34]	15 September 2017	
55	BOSS DR12	0.59	0.481 ± 0.066	[34]	15 September 2017	
56	BOSS DR12	0.64	0.486 ± 0.070	[34]	15 September 2017	
57	SDSS DR7	0.1	0.376 ± 0.038	[35]	12 December 2017	$(\Omega_{0m}, \Omega_b, \sigma_8) = (0.282, 0.046, 0.817)$
58	SDSS-IV	1.52	0.420 ± 0.076	[36]	8 January 2018	$(\Omega_{0m}, \Omega_b h^2, \sigma_8) = (0.26479, 0.02258, 0.8)$
59	SDSS-IV	1.52	0.396 ± 0.079	[37]	8 January 2018	$(\Omega_{0m}, \Omega_b h^2, \sigma_8) = (0.31, 0.022, 0.8225)$
60	SDSS-IV	0.978	0.379 ± 0.176	[38]	9 January 2018	$(\Omega_{0m}, \sigma_8) = (0.31, 0.8)$
61	SDSS-IV	1.23	0.385 ± 0.099	[38]	9 January 2018	
62	SDSS-IV	1.526	0.342 ± 0.070	[38]	9 January 2018	
63	SDSS-IV	1.944	0.364 ± 0.106	[38]	9 January 2018	

Reference: [1] Song & Percival (2009), [2] Tegmark et al. (2006), [3] Davis et al. (2011), [4] Hudson & Turnbull (2013), [5] Turnbull et al. (2012), [6] Samushia et al. (2012), [7] Blake et al. (2012), [8] Beutler et al. (2012), [9] Tojeiro et al. (2012), [10] De La Torre et al. (2013), [11] Chuang & Wang (2013), [12] Komatsu et al. (2011), [13] Blake et al. (2013), [14] Sanchez et al. (2014), [15] Anderson et al. (2014), [16] Howlett et al. (2015), [17] Feix et al. (2015), [18] Tegmark et al. (2004), [19] Okumura et al. (2016), [20] Hinshaw et al. (2013), [21] Chuang et al. (2016), [22] Alam et al. (2017), [23] Beutler et al. (2017), [24] Wilson (2016), [25] Gil-Marín et al. (2017), [26] Hawken et al. (2017), [27] Huterer et al. (2017), [28] De La Torre et al. (2017), [29] Ade et al. (2016), [30] Pezzotta et al. (2017), [31] Feix et al. (2017), [32] Howlett et al. (2017), [33] Mohammad et al. (2018), [34] Wang et al. (2018), [35] Shi et al. (2018), [36] Gil-Marín et al. (2018), [37] Hou et al. (2018), [38] Zhao et al. (2019).

Table A2. The latest Hubble parameter measurements $H(z)$ (in units of $\text{km s}^{-1} \text{Mpc}^{-1}$) and their errors σ_H at redshift z obtained from the differential age method (DA).

Index	z	$H(z)$	σ_H	Reference
1	0.07	69.0	19.6	Zhang et al. (2014)
2	0.12	68.6	26.2	
3	0.2	72.9	29.6	
4	0.28	88.8	36.6	
5	0.1	69	12	
6	0.17	83	8	
7	0.27	77	14	
8	0.4	95	17	
9	0.48	97	60	
10	0.88	90	40	Stern et al. (2010)
11	0.9	117	23	
12	1.3	168	17	
13	1.43	177	18	
14	1.53	140	14	
15	1.75	202	40	
16	0.1797	75	4	
17	0.1993	75	5	
18	0.3519	83	14	
19	0.5929	104	13	Moresco et al. (2012)
20	0.6797	92	8	
21	0.7812	105	12	
22	0.8754	125	17	
23	1.037	154	20	
24	0.3802	83	13.5	
25	0.4004	77	10.2	
26	0.4247	87.1	11.2	Moresco et al. (2016)
27	0.4497	92.8	12.9	
28	0.4783	80.9	9	
29	1.363	160	33.6	
30	1.965	186.5	50.4	Moresco (2015)
31	0.47	89	34	
				Ratsimbazafy et al. (2017)

Table A3. The latest Hubble parameter measurements $H(z)$ (in units of $\text{km s}^{-1} \text{Mpc}^{-1}$) and their errors σ_H at redshift z obtained from the radial BAO method (clustering).

Index	z	$H(z)$	σ_H	Reference
1	0.24	79.69	2.65	Gaztanaga et al. (2009)
2	0.43	86.45	3.68	
3	0.3	81.7	6.22	Oka et al. (2014)
4	0.31	78.17	4.74	
5	0.36	79.93	3.39	
6	0.40	82.04	2.03	
7	0.44	84.81	1.83	
8	0.48	87.79	2.03	
9	0.52	94.35	2.65	
10	0.56	93.33	2.32	
11	0.59	98.48	3.19	
12	0.64	98.82	2.99	
13	0.35	82.7	8.4	
14	0.38	81.5	1.9	
15	0.51	90.4	1.9	Alam et al. (2017)
16	0.61	97.3	2.1	
17	0.44	82.6	7.8	
18	0.6	87.9	6.1	Blake et al. (2012)
19	0.73	97.3	7	
20	0.57	96.8	3.4	
21	2.33	224	8	Anderson et al. (2014)
22	2.34	222	7	
23	2.36	226	8	
				Font-Ribera et al. (2014)